ACS Photonics

Open Access

This article is licensed under CC-BY 4.0

pubs.acs.org/journal/apchd5

Article

Addressing the Optical Degradation of 1.3 μm Quantum Dot Lasers through Subthreshold Characterization

Michele Zenari,* Matteo Buffolo, Carlo De Santi, Justin Norman, Eamonn T. Hughes, John E. Bowers, Robert Herrick, Gaudenzio Meneghesso, Enrico Zanoni, and Matteo Meneghini

Cite This: ACS Photonics 2023, 10, 4188–4195

Read Online

ACCESS | Metrics & More | Article Recommendations

ABSTRACT: We propose a novel methodology capable of separately evaluating the contribution of the different recombination processes in quantum dot laser diodes (QD LDs) driven below-threshold. The proposed approach is based on the analysis of the subthreshold optical characteristics of the devices and was used to evaluate the variation in recombination parameters induced by a long-term stress test. The results of this work indicate that the optical degradation of QD LDs is mainly driven by the increase in the concentration of nonradiative recombination centers within the QWs (quantum wells), with consequent decrease in the injection efficiency. The reported results are of fundamental importance because they demonstrate that conventional models for the extrapolation of the nonradiative lifetime are not capable of reasonably extracting that parameter for LDs featuring a dot-in-a-well-based active region: this limitation is overcome by the reported modeling approach.

KEYWORDS: *degradation, quantum dots, injection efficiency, modeling, silicon photonics*

1. INTRODUCTION

The ever-increasing demand for Internet global traffic has pushed the need for new technologies for high-efficiency and fast communication systems, especially within datacenters.[1] Silicon photonics is one of the most promising technologies in this field since it enables photonic components to be integrated onto a silicon platform. Thanks to silicon and silicon dioxide, which are transparent in the datacom window, it is possible to develop high-index contrast waveguides that can be integrated on silicon substrates.[2]

However, one of the main issues related to the fabrication of photonic-integrated circuits is the integration of light sources. Indeed, silicon is not suitable for fabricating efficient laser diodes (LDs) due to its indirect band gap.[3,4] LDs for silicon photonics are commonly made of III−V compound semiconductors, which are integrated on silicon or silicon-on-insulator (SOI) substrates.[5] As an alternative to such hybrid integration, which requires an accurate laser-chip alignment, heteroepitaxial growth enables growth of III−V materials onto 300 mm diameter Si or SOI platforms,[6] thus providing a scalable and cost-effective growth process. The growth of III−V materials on silicon results in the generation of threading dislocations and antiphase domains, whose origin was ascribed to the lattice constant mismatch and thermal expansion coefficient mismatch among silicon and GaAs.[7] The most promising solution for reducing the sensitivity to semiconductor defects, which worsen both the optical performance and the lifespan of these devices,[8] is to integrate quantum dots (QDs) in the active region. Owing to their three-dimensional confinement of carriers, and to their fast carrier capture rate,[9] QD LDs are less sensitive to the presence of the crystalline defects which are responsible for enhancing the nonradiative recombination rate inside the active region of the devices. The inclusion of QDs inside a QW (in turn surrounded by GaAs barriers) is beneficial not only in terms of carrier confinement (and, therefore, carrier escape) but also in terms of material quality. Indeed, the direct growth of InAs on GaAs could lead to the formation of crystalline defects,[10] whereas the growth on an InGaAs template was found to have a lower contribution of defects due to the lower strain in InAs/InGaAs structures.[11] Recent studies[12] demonstrated that reducing the density of defects in QD lasers heteroepitaxially grown on silicon is of paramount importance for improving both the device efficiency and reliability.

Received: June 28, 2023
Revised: October 27, 2023
Accepted: October 31, 2023
Published: November 11, 2023

Downloaded via 151.51.199.63 on December 27, 2024 at 12:38:34 (UTC).
See https://pubs.acs.org/sharingguidelines for options on how to legitimately share published articles.

ACS Publications

© 2023 The Authors. Published by American Chemical Society

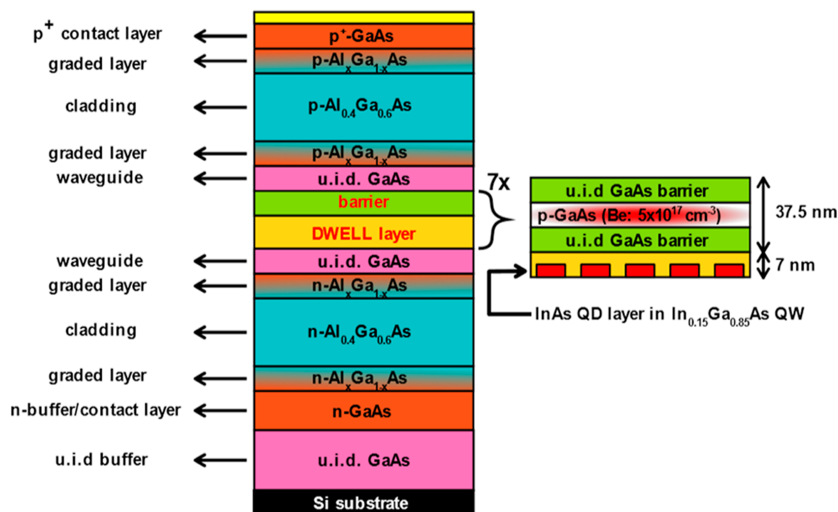

Figure 1. Schematic view of the epitaxial structure of the samples under investigation.

For optimizing the design of QD lasers and for being able to accurately characterize the presence of parasitic recombination processes, specific techniques need to be defined. At the laboratory level, it is desirable that such techniques are based on simple experimental measurements, such as, for instance,—on the analysis of optical power vs current curves, which are accessible to most laboratories.

One of the most common approaches to evaluate the nonradiative lifetime in semiconductor LDs based on simple optical measurements is the van Opdorp method.[13] However, this model is incomplete since (a) it does not consider the role of Auger-Meitner recombination and (b) it is not suitable for modeling the dot-in-a-well (DWELL) structure in which carriers are supplied to QDs by a QW acting as a reservoir.

Within this paper, we propose a novel model based on rate equations that allows the evaluation of the contribution of radiative, Shockley-Read-Hall (SRH), and Auger-Meitner recombination, along with the SRH leakage component in the QWs. Such a methodology is based on the analysis of the subthreshold characteristics of QD lasers and significantly advances the state-of-the-art in this field. We demonstrate the validity of the model through the analysis of the $L-I$ curves of QD LDs with self-assembled InAs QDs embedded in InGaAs QWs designed for 1.3 μm wavelength emission. The results are consistent with previous reports[14] and indicate that the degradation is not promoted by the growth of defects inside the QDs but is rather caused by the increase in nonradiative recombination occurring in the QW.

2. SAMPLES UNDER INVESTIGATION

The devices analyzed within this work are state-of-the-art InAs QD LDs epitaxially grown by MBE (molecular beam epitaxy) on silicon substrates. The samples are designed for emission at 1.3 μm. The epitaxial structure (Figure 1) is formed by a periodic active region enclosed within two GaAs wave-guiding layers and two $Al_{0.4}Ga_{0.6}As$ cladding layers, grown on top of a ~ 3 μm thick GaAs buffer layer. The active region of the lasers is composed of seven equal DWELL layers, each featuring undoped GaAs barriers and a 10 nm thick Be-doped layer ($N_A = 5 \times 10^{17}$ cm^{-3}), separated from the $In_{0.15}Ga_{0.85}As$ well containing the layer of self-assembled InAs QDs, whose areal density is around 5×10^{10} cm^{-2} (further details on the growth processes can be found in ref 15). The processing of the devices was then completed with the etching of the 2.5 μm wide ridge, the thinning of the silicon substrate, and the cleavage of the facets that form a 1350 μm long Fabry-Pérot optical cavity.

3. EXPERIMENTAL METHODS

For our experimental purposes, one representative device with threading dislocation density (TDD) equal to 7×10^7 cm^{-2} has been stressed and characterized on-wafer. Temperature control was achieved by means of a TEC-controlled baseplate. The electrical supply was provided by a source meter, connected to the device in a four-wire (Kelvin) configuration. The optical measurements were carried out using an amplified Ge photodiode. The stress experiment was interrupted at different stages to evaluate the effects of device degradation by carrying out optical power versus current ($L-I$) characterization. Both stress and characterization were carried out at a fixed baseplate temperature of T_{AMB} = 35 °C. Based on previous results on similar devices[14,16] (TDD = 7×10^6 cm^{-2}, three QD layers), a constant stress current of 202.5 mA (5 kA/cm^2) was chosen in order to induce a sufficient amount of degradation in a time frame of 500 h (about 3 weeks).[17]

4. RESULTS AND DISCUSSION

4.1. Modeling of Optical Degradation—Model Definition. The variation of the $L-I$ characteristics exhibited by the device during the aging procedure is shown in Figure 2a:

The reported curves show a decrease in the slope efficiency (SE), an increase of the threshold current (I_{th}), and a decrease in the subthreshold emission (OP_{sub}). The faster degradation of the optical characteristics shown in Figure 2a occurring within the first 2000−5000 min is compatible with a square root dependence on stress time (see inset of Figure 2b).[16] This feature suggests a diffusion process (regulated by Fick's second law of diffusion[18]) which can be interpreted with the migration of defects/impurities in the active region worsening the optical performance, as described in our previous study on similar devices.[14] Consistent with prior experiments,[14,19] the relative variations of I_{th} and OP_{sub} appear to be linearly correlated (Figure 2b), indicating that a common degradation process is affecting both parameters at the same time. Based on this observation, we developed a methodology for analyzing the recombination dynamics, which is based on the study of the

https://doi.org/10.1021/acsphotonics.3c00910
ACS Photonics 2023, 10, 4188−4195

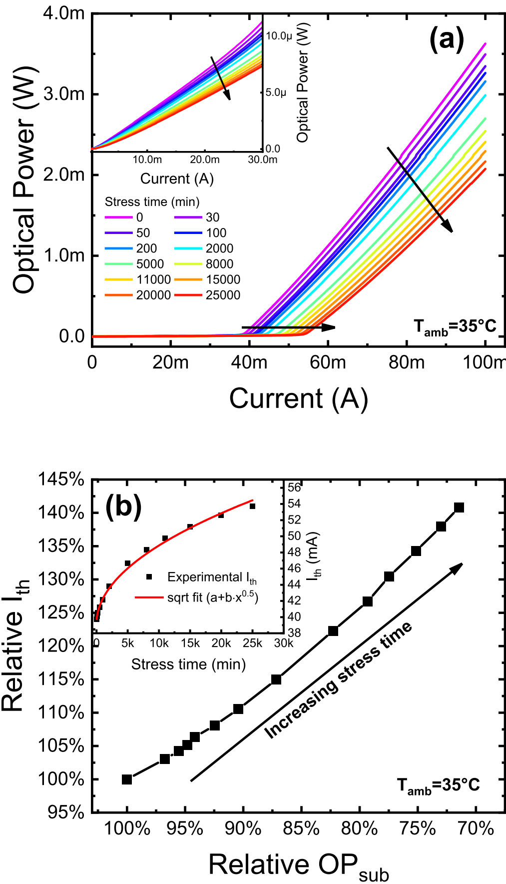

Figure 2. (a) Variation of the $L-I$ curves during the constant current stress: we can observe an increase in threshold current, a decrease in the slope efficiency, and decrease in subthreshold emission. (b) Correlation between threshold current and subthreshold emission.

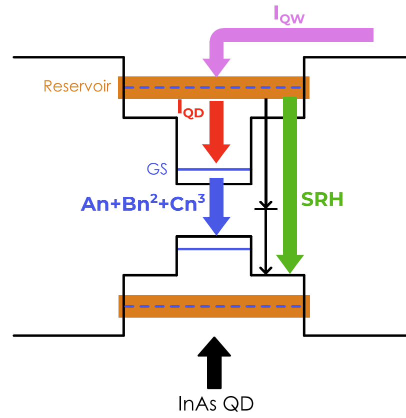

Figure 3. Schematic representation of the main recombination processes occurring in the subthreshold regime: the input current feeds the InGaAs QW, which is supposed to act as a carrier reservoir for the QDs. Carrier within the QW can also be lost through SRH recombination rates taken into account.

optical degradation below threshold. This choice is justified by the fact that a comprehensive modeling of the optical characteristics above threshold would have strongly increased the number of fitting parameters required to describe the theoretical behavior of the device (see for example refs 20 and 21). Considering that many of these parameters cannot be experimentally or theoretically determined with reasonable accuracy, this would have ultimately increased the degrees of freedom of the model, thus, lowering the level of confidence of the results. To numerically describe the optical emission below I_{th}, we considered the simplified recombination scheme reported in Figure 3.

At first, we assumed that the input current (I_{QW}) feeds entirely the QWs, which act as carrier reservoirs for the QDs, thus neglecting possible carrier escape/overflow processes. Carrier losses within the QWs are accounted for by a SRH recombination term, which mainly represents the effects of the nonradiative recombination centers (NRRCs) located in the InGaAs QW that subtract carriers from the reservoir.[22] With regard to the QDs, we consider only the ground state (GS)-related emission and recombination processes since in the subthreshold regime, the current densities are low enough to allow GS to be much more populated than ES1 (first excited state).[23] In Figure 3, the rate at which carriers are fed to the QD GS from the reservoir is represented by I_{QD}, whereas the recombination processes describing carrier dynamics within the QD itself are described by the coefficients A (SRH recombination), B (spontaneous emission), and C (Auger-Meitner recombination). Also for the QDs, we do not consider any escape process. Based on previous considerations, the recombination dynamics within the system shown in Figure 3 can be represented by a set of two differential equations

$$\begin{cases} \dfrac{dN_{well}}{dt} = \dfrac{I}{qV_{well}} - \dfrac{N_{well}}{\tau_{nr}} - \dfrac{I_{QD}}{qV_{QD}} \\ \dfrac{dN_{QD}}{dt} = \dfrac{I_{QD}}{qV_{QD}} - AN_{QD} - BN_{QD}^2 - CN_{QD}^3 \end{cases} \tag{1}$$

where N_{well} is the carrier density in the QWs, NQD is the carrier density in the QDs, V_{well} is the volume of the InGaAs wells, V_{QD} is the total volume of the QDs, and τ_{nr} represents the nonradiative lifetime inside the QWs. In eq 1, the first equation represents the QW rate equation, whereas the second one describes recombination within the QDs. In steady-state conditions ($dN_{well}/dt = 0$ and $dN_{QD}/dt = 0$), we can write

$$\begin{cases} 0 = \dfrac{I}{qV_{well}} - \dfrac{N_{well}}{\tau_{nr}} - \dfrac{I_{QD}}{qV_{QD}} \Rightarrow \\ \Rightarrow \dfrac{I}{qV_{well}} = \dfrac{N_{well}}{\tau_{nr}} + \dfrac{I_{QD}}{qV_{QD}} \\ 0 = \dfrac{I_{QD}}{qV_{QD}} - AN_{QD} - BN_{QD}^2 - CN_{QD}^3 \Rightarrow \\ \Rightarrow \dfrac{I_{QD}}{qV_{QD}} = AN_{QD} + BN_{QD}^2 + CN_{QD}^3 \end{cases} \tag{2}$$

By combining the two equations, we obtain

$$\frac{I}{qV_{well}} = \frac{N_{well}}{\tau_{nr}} + AN_{QD} + BN_{QD}^2 + CN_{QD}^3 \tag{3}$$

Now we assume that the number of photons generated in the active region (L) through spontaneous emission, per unit of time, is determined by the following relation

$$L = V_{QD}BN_{QD}^2 \tag{4}$$

https://doi.org/10.1021/acsphotonics.3c00910
ACS Photonics 2023, 10, 4188−4195

Second, we hypothesize that the amount of photons emitted outside the laser per unit of time (L_{ext}) is proportional to the rate of photons generated in the active region divided by a term called extraction efficiency (E), which takes into account the contribution of absorption, diffraction, mode coupling, and collection losses that limit the fraction of output light that can be actually measured ($L = L_{ext}/E$). The carrier density in the QDs can therefore be determined by

$$N_{QD} = \sqrt{\frac{L}{BV_{QD}}} = \sqrt{\frac{L_{ext}}{EBV_{QD}}} \tag{5}$$

By substituting eq 5 into (3), we obtain

$$\frac{I}{qV_{well}} = \frac{N_{well}}{\tau_{nr}} + A\sqrt{\frac{L_{ext}}{EBV_{QD}}} + \frac{L_{ext}}{V_{QD}\cdot E} + C\left(\frac{L_{ext}}{EBV_{QD}}\right)^{3/2} \tag{6}$$

The external quantum efficiency (η_{ext}) can then be calculated as

$$\eta_{ext} = \frac{qL_{ext}}{I} = \frac{q\cdot L_{ext}}{q\left(V_{well}\frac{N_{well}}{\tau_{nr}} + V_{well}A\sqrt{\frac{L_{ext}}{EBV_{QD}}} + \frac{V_{well}}{V_{QD}\cdot E}L_{ext} + V_{well}C\left(\frac{L_{ext}}{EBV_{QD}}\right)^{3/2}\right)} \tag{7}$$

Finally, the inverse of the external quantum efficiency can be written as

$$\frac{1}{\eta_{ext}} = V_{well}\frac{N_{well}}{\tau_{nr}}\frac{1}{L_{ext}} + \frac{V_{well}}{V_{QD}\cdot E} + V_{well}A\sqrt{\frac{1}{EBV_{QD}}}\sqrt{\frac{1}{L_{ext}}} + V_{well}C\left(\frac{1}{EBV_{QD}}\right)^{3/2}\sqrt{L_{ext}} \tag{8}$$

This final equation describes $1/\eta_{ext}$ as a function of $1/L_{ext}$ similar to the van Opdorp method, where L_{ext} can be derived from experimental measurements by dividing the optical power of the $L-I$ curves by the photon energy ($L_{ext} = \mathrm{OP}/h\nu$).

4.2. Modeling of Optical Degradation—Model Validation. Based on eq 8, we fitted the experimentally determined $1/\eta_{ext}$ vs $\mathrm{OP}/h\nu$ plots acquired during the stress test. The results of the fit are shown in Figure 4:

The constraints for the fitting are listed in Table 1:

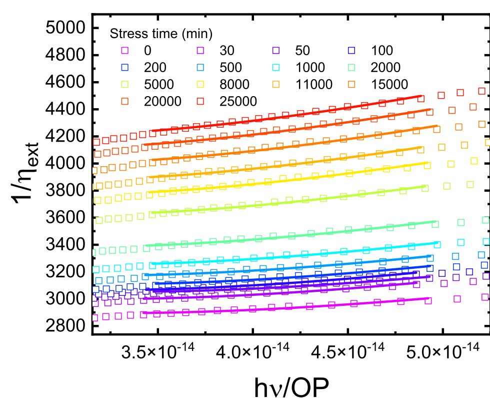

Figure 4. Figure shows the inverse of the external quantum efficiency as a function of the emitted optical power. The inset graph shows the fitting result for each curve collected during the stress procedure.

Table 1. List of Coefficients Used to Fit the Experimental $L-I$ Curves below Threshold

parameter	value	description
V_{well}	1.65×10^{-10} cm^3	InGaAs well volume
V_{QD}	4.72×10^{-11} cm^3	InAs quantum dot volume
A	1×10^{-7} s^{-1}	InAs SRH recombination coefficient[27]
B	1.1×10^{-10} cm^3 s^{-1}	InAs radiative recombination coefficient[24]
C	1×10^{-27} cm^6 s^{-1}	InAs QDs Auger-Meitner recombination coefficient[25,26]
E	fitting param.	extraction efficiency
N_{well}/τ_{nr}	fitting param. cm^{-3} s^{-1}	SRH recombination rate (QWs)

Since QDs are sandwiched between the wetting layer and the InGaAs well, to determine V_{QD}, we assumed that in the 7 nm InGaAs well, an equivalent 2 nm layer of InAs QDs was placed in the middle of the DWELL. Actually, the real QD volume should be lower as QDs do not form a continuous layer, but from a dot to another, there is a little distance in between. In Figure 4, data were fitted from 9.5 to 13.5 mA, a bias range we opted for to evaluate the model enough below the lasing threshold, in order to avoid as much as possible the contribution of the stimulated emission to the detected light output. After calculating N_{well}/τ_{nr} from each $L-I$ curve, we estimated the SRH leakage current (first term of eq 8) in the QWs and compared the trend with the subthreshold emission extrapolated within the same bias range of the fitting.

Figure 5 shows that the degradation of the OP_{sub} and the increase in the SRH leakage current are linearly correlated,

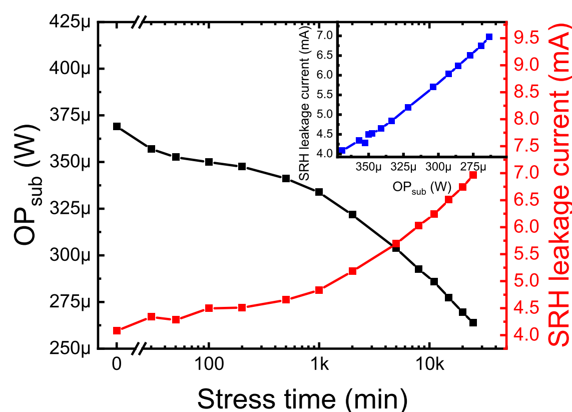

Figure 5. Red curve represents the resulting SRH leakage current from the fit of each curve collected during the stress. The inset shows that there is a linear correlation between the degradation of the subthreshold emission and the trend of the SRH current.

indicating that the proposed model effectively describes the evolution of the $L-I$ characteristics below threshold as the increase in QW loss current explains the radiative efficiency drop below threshold, thus reproducing the optical degradation. Despite that, if we look in more detail to the fitting results shown in Figure 4, we can see that the fitted curves tend to tilt upward for high bias currents, i.e., for high OP levels, with respect to the experimental data. This can be explained by considering that the model does not take into account the stimulated recombination: for this reason, when current is increased, the predicted increase in $1/\eta_{ext}$ (decrease in η_{ext}) due to the Auger-Meitner term (proportional to $L_{ext}^{-1/2}$) is not compensated by any term related to stimulated emission. This would tilt the same curve

https://doi.org/10.1021/acsphotonics.3c00910
ACS Photonics 2023, 10, 4188−4195

downward since stimulated emission is a much faster process with respect to spontaneous emission (in reasonable bias and photon-density conditions).

4.3. Interpretation of the Optical Degradation. According to the proposed model, the degradation of the optical characteristics below threshold is driven by the increase in carrier losses in the QWs, possibly due to the increase in NRRCs within this region.[16,19,28−31] To link this behavior with the degradation of the optical characteristics above threshold, i.e., to the increase in I_{th} and the decrease in SE, we employed a second modified rate equation model to qualitatively analyze the variation of the $L-I$ curves. The proposed model is valid for a QW laser, but the phenomenological considerations can be applied also to QD lasers.[35] The set of carrier and photon rate equations is the following

$$\begin{cases} \frac{dN}{dt} = \frac{\eta_{inj} I}{qV} - N(A + BN + CN^2) - g_0(N - N_{tr}) \frac{S}{1+EPS\cdot S} \\ \frac{dS}{dt} = \Gamma g_0(N - N_{tr})\frac{S}{1+EPS\cdot S} - \frac{S}{t_p} + \Gamma\beta BN^2 \end{cases} \quad (9)$$

where S is the photon density, and all remaining parameters are described in Table 2. We chose to adopt such values according to papers involving QD LDs in order to describe a plausible QD LD with similar characteristics to our devices.

Table 2. List of Parameters Employed to Model the Optical Characteristics above Threshold

symbol	description	value	unit	ref.
q	electron charge	1.6×10^{-19}	[C]	
V	active volume	4.67×10^{-11}	[cm^3]	
$A = \frac{1}{\tau_{SRH}}$	SRH coeff.	$1/1 \times 10^{-9}$	[s^{-1}]	
B	radiative coeff.	1.1×10^{-10}	[cm^3 s^{-1}]	24
C	Auger-Meitner coeff.	1×10^{-27}	[cm^6 s^{-1}]	
g_0	gain slope constant	0.926×10^{-5}	[cm^{-3} s^{-1}]	36
N_{tr}	transparency carrier density	1×10^{18}	[cm^{-3}]	37
EPS	gain compression factor	1×10^{-17}	[cm^3]	36
Γ	confinement factor	0.02		38
τ_p	photon lifetime	8.56×10^{-12}	[s]	39
β	spontaneous emission factor	1×10^{-4}		38
η_{inj}	injection efficiency	0.87		39

To incorporate the contribution of the SRH leakage current affecting the DWELLs into the simplified model described in eq 9, we included the apparent injection efficiency coefficient η_{inj}. In this case, η_{inj} can be defined as the ratio of radiative recombination rate per unit volume (i.e., the QD volume) over the rate at which carriers are injected into the device. The leakage current in the QWs is affecting the fraction of carriers being injected into the QDs; therefore, an injection efficiency term can effectively model this kind of phenomenon. To model the observed optical degradation, we simulated two distinct scenarios: (i) the increase in the SRH recombination rate in the active layers and (ii) a lowering of η_{inj}.

- (i) An increase the SRH recombination rate in the active layers (i.e., a decrease in the SRH lifetime) lowers the differential gain at a given bias current as the SRH component is subtracting carriers from the radiative processes; therefore, the device will reach the threshold at higher currents. As shown by Figure 6a, this phenomenon can explain the worsening of the I_{th} and of the OP_{sub}, but not the decrease in SE, since this parameter should remain unaffected by the increment of the nonradiative recombination in the active layers, as the carrier density in the active layers is the same with varying the A coefficient. The demonstration that SE depends on η_{inj} but not on A is reported in Appendix A.

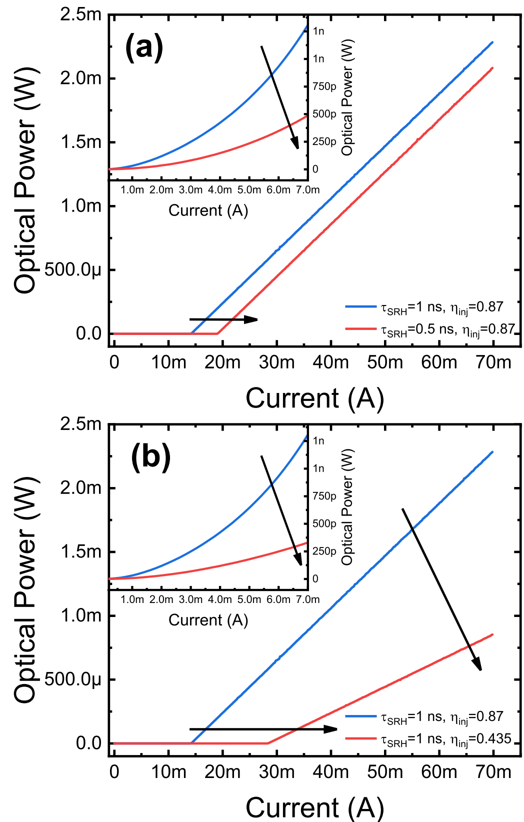

Figure 6. (a) $L-I$ curves as a function of τ_{SRH}: worsening of I_{th} and OP_{sub}. (b) $L-I$ curves as a function of η_{inj}: worsening of I_{th}, OP_{sub}, and SE.

- (ii) When lowering η_{inj}, the carrier density in the active layers is lowered as an increasing part of the input current is lost through other nonradiative processes. Therefore, to reach lasing threshold, the device will require more current to compensate for the increased carrier losses. Since the SE is directly correlated to the external differential quantum efficiency, it represents the increment of coherent photons coming out of device per second with respect to the increment in the number of carriers injected in the laser in the same time interval. If some carriers are lost due to nonradiative processes (the QW loss in QD LDs decreases the injection efficiency inside QDs), the SE is also affected. Indeed, the SE can be defined as[40]

$$SE = \eta_{inj}\frac{\alpha_{mirror}}{\alpha_{mirror} + \alpha_{internal}}\frac{h\nu}{q} = \eta_{ext}\frac{h\nu}{q} \quad (10)$$

https://doi.org/10.1021/acsphotonics.3c00910
ACS Photonics 2023, 10, 4188−4195

where α_{mirror} and $\alpha_{internal}$ are, respectively, the mirror and internal losses, q is the fundamental charge, h is Planck's constant, and ν is the frequency.

Based on these considerations, and on the experimental results in,[16,19] the optical degradation of QD LDs has to be modeled by considering a reduction in the injection efficiency. This reduction can be ascribed to the increase in carrier losses within the DWELL, which is mainly driven by the increase of defects close to the InGaAs well,[28,29,32,33] which are responsible of enhancing the carrier losses affecting the QD reservoir (Figure 5). According to previous investigations, the origin of the defects contributing to the increase in SRH recombination could be related to point defects participating to the recombination enhanced growth of pre-existent misfit dislocations,[28,29] such as As_{Ga} or V_{As},[16,34] or, in general, to the extended defects themselves.

5. CONCLUSIONS

In summary, with this work, we developed a novel model that allows us to estimate the relative variation of the loss current, associated with SRH recombination in the well, during the aging of 1.3 μm QD LDs grown on silicon by the $L-I$ characteristics below threshold. The outcome of our modeling confirmed that the optical degradation of the LDs is mainly caused by the increase in the NRRCs inside the InGaAs well. Our hypothesis is supported by the qualitative simulation of the optical characteristics above the threshold which demonstrates that the increase in the rate of SRH recombination inside QDs is not sufficient to explain the degradation of these devices, whereas lowering of the injection efficiency (which represents the increase of QW loss current) confirms the previous experimental results. The methodology proposed in this work can be useful also to QD LDs based on other materials, such as InGaN/GaN QD LDs featuring the DWELL structure.[41,42] Our approach can be applied as long as the degradation is dominated by lowering the injection efficiency over the decreases in the radiative efficiency in QDs.

APPENDIX A

Dependence of the Slope Efficiency on η_{inj} and A

In this appendix, we show in which way SE is affected by η_{inj} and A. For the sake of simplicity, we can rewrite the first of the two equations in the system of eq 9 as

$$\frac{dN}{dt} = \frac{\eta_{inj} I}{qV} - \frac{N}{\tau} - S v_g g \tag{11}$$

where τ is the reciprocal of $A + BN + CN^2$, v_g is the group velocity, and g is the material gain. If we consider eq 11 around threshold (thus neglecting the second term on the right-hand side of the equation) in steady-state conditions, we can write

$$\frac{\eta_{inj} I_{th}}{qV} = \frac{N_{th}}{\tau} \Rightarrow N_{th} = \frac{\tau \eta_{inj} I_{th}}{qV} \tag{12}$$

Substituting N_{th} in eq 11 yields

$$\frac{dN}{dt} = \frac{\eta_{inj}(I - I_{th})}{qV} - S v_g g \tag{13}$$

In steady-state condition, the photon density S can be expressed as

$$S = \frac{\eta_{inj}(I - I_{th})}{qVv_g g} \tag{14}$$

by multiplying the photon density, S, by the energy per photon, $h\nu$, and the cavity volume, V_p, we obtain the stored optical energy in the cavity E_{os} $(S \cdot h\nu \cdot V_p)$. Then, by multiplying E_{os} by the energy loss rate through the mirrors $v_g \alpha_m = 1/\tau_m$, which is the product of the group velocity and the mirror losses, we obtain the optical power output from the mirrors

$$P_{out} = \frac{h\nu S V_p}{\tau_m} \tag{15}$$

Finally, the SE can be obtained from the derivative of the output power with respect to the current

$$\begin{aligned} SE &= \frac{dP_{out}}{dI} = \frac{d}{dI}\left(\frac{h\nu S V_p}{\tau_m}\right) \\ &= \frac{d}{dI}\left(\frac{h\nu V_p}{\tau_m}\frac{\eta_{inj}(I - I_{th})}{qVv_g g}\right) = \frac{h\nu V_p}{\tau_m}\frac{\eta_{inj}}{qVv_g g} \end{aligned} \tag{16}$$

From this last equation, we can notice that the SE does not depend on the carrier lifetime τ, accounting for the values of the ABC coefficients, which impacts on the value of I_{th}.[40] Therefore, eq 16 shows that SE depends on η_{inj} but not on A.

AUTHOR INFORMATION

Corresponding Author

Michele Zenari − *Department of Information Engineering, University of Padova, Padova 35131, Italy*; orcid.org/0000-0001-8803-3824; Email: zenarimich@dei.unipd.it

Authors

Matteo Buffolo − *Department of Information Engineering, University of Padova, Padova 35131, Italy*

Carlo De Santi − *Department of Information Engineering, University of Padova, Padova 35131, Italy*

Justin Norman − *Department of Electrical and Computer Engineering, University of California, Santa Barbara, California 93106, United States*

Eamonn T. Hughes − *Department of Electrical and Computer Engineering, University of California, Santa Barbara, California 93106, United States*; orcid.org/0000-0003-2428-6923

John E. Bowers − *Department of Electrical and Computer Engineering and Materials Department, University of California, Santa Barbara, California 93106, United States*

Robert Herrick − *Formerly with Intel Corporation, Santa Clara, California 95054, United States*

Gaudenzio Meneghesso − *Department of Information Engineering, University of Padova, Padova 35131, Italy*

Enrico Zanoni − *Department of Information Engineering, University of Padova, Padova 35131, Italy*

Matteo Meneghini − *Department of Information Engineering, University of Padova, Padova 35131, Italy; Department of Physics and Astronomy, University of Padova, Padova 35131, Italy*

Complete contact information is available at: https://pubs.acs.org/10.1021/acsphotonics.3c00910

https://doi.org/10.1021/acsphotonics.3c00910
ACS Photonics 2023, 10, 4188−4195

Notes

The authors declare no competing financial interest.

ACKNOWLEDGMENTS

This work was supported in part by the U.S. Defense Advanced Research Project Agency (DARPA) LUMOS program.

REFERENCES

(1) Patterson, D.; De Sousa, I.; Archard, L.-M. The Future of Packaging with Silicon Photonics. *Chip Scale Rev.* **2017**, 1−10.
(2) Bogaerts, W.; Chrostowski, L. Silicon Photonics Circuit Design: Methods, Tools and Challenges. *Laser Photonics Rev.* **2018**, *12* (4), 1−29.
(3) Trupke, T.; Green, M. A.; Würfel, P. Optical Gain in Materials with Indirect Transitions. *J. Appl. Phys.* **2003**, *93* (11), 9058−9061.
(4) Chen, M. J.; Tsai, C. S.; Wu, M. K. Optical Gain and Co-Stimulated Emissions of Photons and Phonons in Indirect Bandgap Semiconductors. *Japanese Journal of Applied Physics, Part 1: Regular Papers and Short Notes and Review Papers.* **2006**, *45* (8B), 6576−6588.
(5) Stojanović, V.; Ram, R. J.; Popović, M.; Lin, S.; Moazeni, S.; Wade, M.; Sun, C.; Alloatti, L.; Atabaki, A.; Pavanello, F.; Mehta, N.; Bhargava, P. Monolithic Silicon-Photonic Platforms in State-of-the-Art CMOS SOI Processes [Invited]. *Opt. Express* **2018**, *26* (10), 13106.
(6) Shang, C.; Feng, K.; Hughes, E. T.; Clark, A.; Debnath, M.; Koscica, R.; Leake, G.; Herman, J.; Harame, D.; Ludewig, P.; Wan, Y.; Bowers, J. E. Electrically Pumped Quantum-Dot Lasers Grown on 300 Mm Patterned Si Photonic Wafers. *Light Sci. Appl.* **2022**, *11* (1), 299.
(7) Norman, J. C.; Zhang, Z.; Jung, D.; Shang, C.; Kennedy, M.; Dumont, M.; Herrick, R. W.; Gossard, A. C.; Bowers, J. E. The Importance of P-Doping for Quantum Dot Laser on Silicon Performance. *IEEE J. Quantum Electron.* **2019**, *55* (6), 1−11.
(8) Jung, D.; Herrick, R.; Norman, J.; Turnlund, K.; Jan, C.; Feng, K.; Gossard, A. C.; Bowers, J. E. Impact of Threading Dislocation Density on the Lifetime of InAs Quantum Dot Lasers on Si. *Appl. Phys. Lett.* **2018**, *112* (15), 153507.
(9) Sun, K. W.; Chen, J. W.; Lee, B. C.; Lee, C. P.; Kechiantz, A. M. Carrier Capture and Relaxation in InAs Quantum Dots. *Nanotechnology* **2005**, *16* (9), 1530−1535.
(10) Lin, S. W.; Balocco, C.; Missous, M.; Peaker, A. R.; Song, A. M. Coexistence of Deep Levels with Optically Active InAs Quantum Dots. *Phys. Rev. B Condens. Matter Mater. Phys.* **2005**, *72* (16), 165302.
(11) Golovynskyi, S.; Seravalli, L.; Datsenko, O.; Trevisi, G.; Frigeri, P.; Gombia, E.; Golovynska, I.; Kondratenko, S. V.; Qu, J.; Ohulchanskyy, T. Y. Comparative Study of Photoelectric Properties of Metamorphic InAs/InGaAs and InAs/GaAs Quantum Dot Structures. *Nanoscale Res. Lett.* **2017**, *12* (1), 335.
(12) Zenari, M.; Buffolo, M.; De Santi, C.; Shang, C.; Hughes, E.; Wan, Y.; Herrick, R. W.; Meneghesso, G.; Zanoni, E.; Bowers, J.; Meneghini, M. Impact of a Defect Trapping Layer on the Reliability of 1.3 Mm Quantum Dot Laser Diodes Grown on Silicon. *Microelectron. Reliab.* **2022**, *138*, 114714.
(13) Van Opdorp, C.; 't Hooft, G. W. Method for Determining Effective Nonradiative Lifetime and Leakage Losses in Double-Heterostructure Lasers. *J. Appl. Phys.* **1981**, *52*, 3827−3839.
(14) Buffolo, M.; Samparisi, F.; Rovere, L.; De Santi, C.; Jung, D.; Norman, J.; Bowers, J. E.; Herrick, R. W.; Meneghesso, G.; Zanoni, E.; Meneghini, M. Investigation of Current-Driven Degradation Grown on Silicon. *IEEE J. Sel. Top. Quantum Electron.* **2020**, *26* (2), 1.
(15) Jung, D.; Norman, J.; Kennedy, M. J.; Shang, C.; Shin, B.; Wan, Y.; Gossard, A. C.; Bowers, J. E. High Efficiency Low Threshold Current 1.3 Mm InAs Quantum Dot Lasers on on-Axis (001) GaP/Si. *Appl. Phys. Lett.* **2017**, *111* (12), 122107.
(16) Buffolo, M.; Lain, F.; Zenari, M.; De Santi, C.; Norman, J.; Bowers, J. E.; Herrick, R. W.; Meneghesso, G.; Zanoni, E.; Meneghini, M. Origin of the Diffusion-Related Optical Degradation of 1.3 μm Inas QD-LDs Epitaxially Grown on Silicon Substrate. *IEEE J. Sel. Top. Quantum Electron.* **2022**, *28* (1: Semiconductor Lasers), 1−9.
(17) Beanland, R.; Sánchez, A. M.; Childs, D.; Groom, K. M.; Liu, H. Y.; Mowbray, D. J.; Hopkinson, M. Structural Analysis of Life Tested 1.3 μm Quantum Dot Lasers. *J. Appl. Phys.* **2008**, *103* (1), 014913.
(18) Orita, K.; Meneghini, M.; Ohno, H.; Trivellin, N.; Ikedo, N.; Takigawa, S.; Yuri, M.; Tanaka, T.; Zanoni, E.; Meneghesso, G. Analysis of Diffusion-Related Gradual Degradation of InGaN-Based Laser Diodes. *IEEE J. Quantum Electron.* **2012**, *48* (9), 1169−1176.
(19) Buffolo, M.; Samparisi, F.; De Santi, C.; Jung, D.; Norman, J.; Bowers, J. E.; Herrick, R. W.; Meneghesso, G.; Zanoni, E.; Meneghini, M. Physical Origin of the Optical Degradation of InAs Quantum Dot Lasers. *IEEE J. Quantum Electron.* **2019**, *55* (3), 1−7.
(20) Rossetti, M.; Bardella, P.; Gioannini, M.; Montrosset, I. Carrier Transport Effects in Multi Layer Quantum Dot Lasers and SLDs. *ECIO'08 Eindhoven—Proc. 14th Eur. Conf. Integr. Opt. Technol. Exhib. Contrib. Invit. Pap.*, 2008; pp 221−224.May 2014.
(21) Zhou, Y.; Duan, J.; Grillot, F.; Wang, C. Optical Noise of Dual-State Lasing Quantum Dot Lasers. *IEEE J. Quantum Electron.* **2020**, *56* (6), 1−7.
(22) Röhm, A.; Lüdge, K.; Schöll, E. *Dynamic Scenarios in Two-State Quantum Dot Lasers: Excited State Lasing, Ground State Quenching, and Dual-Mode Operation*; Springer Science+Business Media, 2015.
(23) Korenev, V. V.; Savelyev, A. V.; Zhukov, A. E.; Omelchenko, A. V.; Maximov, M. V. Analytical Approach to the Multi-State Lasing Phenomenon in Quantum Dot Lasers. *Appl. Phys. Lett.* **2013**, *102* (11), 5−10.
(24) GeFmont, B. L.; Sokolova, Z. N.; Yassievich, I. N. *Sov. Phys. Semicond.* **1982**, *16*, 592−600.
(25) Ghosh, S.; Bhattacharya, P.; Stoner, E.; Singh, J.; Jiang, H.; Nuttinck, S.; Laskar, J. Temperature-Dependent Measurement of Auger Recombination in Self-Organized In0.4Ga0.6As/GaAs Quantum Dots. *Appl. Phys. Lett.* **2001**, *79* (6), 722−724.
(26) Novikov, I. I.; Gordeev, N. Y.; Maksimov, M. V.; Shernyakov, Y. M.; Semenova, E. S.; Vasil'Ev, A. P.; Zhukov, A. E.; Ustinov, V. M.; Zegrya, G. G. Temperature Dependence of the Effective Coefficient of Auger Recombination in 1.3 Mm InAs/GaAs QD Lasers. *Semicond.* **2005**, *39* (4), 481−484.
(27) Krishnamurthy, S.; Berding, M. A. Full-band-structure calculation of Shockley−Read−Hall recombination rates in InAs. *Full-Band-Structure Calculation of Shockley-Read-Hall Recombination Rates in InAs. J. Appl. Phys.* **2001**, *90* (2), 848−851.
(28) Selvidge, J.; Norman, J.; Salmon, M. E.; Hughes, E. T.; Bowers, J. E.; Herrick, R.; Mukherjee, K. Non-Radiative Recombination at Dislocations in InAs Quantum Dots Grown on Silicon. *Appl. Phys. Lett.* **2019**, *115* (13), 131102.
(29) Selvidge, J.; Hughes, E. T.; Norman, J. C.; Shang, C.; Kennedy, M. J.; Dumont, M.; Netherton, A. M.; Zhang, Z.; Herrick, R. W.; Bowers, J. E.; Mukherjee, K. Reduced Dislocation Growth Leads to Long Lifetime InAs Quantum Dot Lasers on Silicon at High Temperatures. *Appl. Phys. Lett.* **2021**, *118* (19), 192101.
(30) Liu, Z.; Martin, M.; Baron, T.; Chen, S.; Seeds, A.; Penty, R.; White, I.; Liu, H.; Hantschmann, C.; Tang, M.; Lu, Y.; Park, J. S.; Liao, M.; Pan, S.; Sanchez, A.; Beanland, R. Origin of Defect Tolerance in InAs/GaAs Quantum Dot Lasers Grown on Silicon. *J. Light. Technol.* **2020**, *38* (2), 240−248.
(31) Liu, J.; Tang, M.; Deng, H.; Shutts, S.; Wang, L.; Smowton, P. M.; Jin, C.; Chen, S.; Seeds, A.; Liu, H. Theoretical Analysis and Modelling of Degradation for III-V Lasers on Si. *J. Phys. D Appl. Phys.* **2022**, *55* (40), 404006.
(32) Blood, P. Quantum Efficiency of Quantum Dot Lasers. *IEEE J. Sel. Top. Quantum Electron.* **2017**, *23* (6), 1−8.
(33) Shutts, S.; Allford, C. P.; Spinnler, C.; Li, Z.; Sobiesierski, A.; Tang, M.; Liu, H.; Smowton, P. M. Degradation of III-v Quantum Dot Lasers Grown Directly on Silicon Substrates. *IEEE J. Sel. Top. Quantum Electron.* **2019**, *25* (6), 1−6.
(34) Zenari, M.; Buffolo, M.; De Santi, C.; Norman, J.; Meneghesso, G.; Bowers, J. E.; Zanoni, E.; Meneghini, M. Identification of Dislocation-Related and Point-Defects in III-As Layers for Silicon Photonics Applications. *J. Phys. D Appl. Phys.* **2021**, *54* (28), 285101.

https://doi.org/10.1021/acsphotonics.3c00910
ACS Photonics 2023, 10, 4188−4195

(35) Cartledge, J. C.; Srinivasan, R. C. Extraction of DFB Laser Rate Equation Parameters for System Simulation Purposes. *J. Light. Technol.* **1997**, *15* (5), 852−860.
(36) Fiore, A.; Markus, A. Differential Gain and Gain Compression in Quantum-Dot Lasers. *IEEE J. Quantum Electron.* **2007**, *43* (4), 287−294.
(37) Wada, K.; Yoshioka, H.; Zhu, J.; Matsuyama, T.; Horinaka, H. Simple Form of Multimode Laser Diode Rate Equations Incorporating the Band Filling Effect. *Opt. Express* **2011**, *19* (4), 3019.
(38) Saldutti, M.; Tibaldi, A.; Cappelluti, F.; Gioannini, M. Impact of Carrier Transport on the Performance of QD Lasers on Silicon: A Drift-Diffusion Approach. *Photonics Res.* **2020**, *8* (8), 1388.
(39) Jung, D.; Zhang, Z.; Norman, J.; Herrick, R.; Kennedy, M. J.; Patel, P.; Turnlund, K.; Jan, C.; Wan, Y.; Gossard, A. C.; Bowers, J. E. Highly Reliable Low-Threshold InAs Quantum Dot Lasers on On-Axis (001) Si with 87% Injection Efficiency. *ACS Photonics* **2018**, *5* (3), 1094−1100.
(40) Coldren, L. A. Diode Lasers and Photonic Integrated Circuits. *Opt. Eng.* **1997**, *36* (2), 616.
(41) Zhang, M.; Banerjee, A.; Lee, C. S.; Hinckley, J. M.; Bhattacharya, P. A InGaN/GaN Quantum Dot Green (λ=524 nm) Laser. *Appl. Phys. Lett.* **2011**, *98* (22), 221104.
(42) Frost, T.; Banerjee, A.; Sun, K.; Chuang, S. L.; Bhattacharya, P. InGaN/GaN Quantum Dot Red Λ=630 nm Laser. *IEEE J. Quantum Electron.* **2013**, *49* (11), 923−931.

https://doi.org/10.1021/acsphotonics.3c00910
ACS Photonics 2023, 10, 4188−4195